A Comparative NMR Study of the Polypeptide Backbone Dynamics of Hemoglobin in the Deoxy and Carbonmonoxy Forms†

Xiang-jin Song, Yue Yuan,‡ Virgil Simplaceanu, Sarata Chandra Sahu, Nancy T. Ho, and Chien Ho*

Department of Biological Sciences, Carnegie Mellon University, Pittsburgh, Pennsylvania 15213

Received December 27, 2006; Revised Manuscript Received March 30, 2007

ABSTRACT: Model-free-based NMR dynamics studies have been undertaken for polypeptide backbone amide N−H bond vectors for both the deoxy and carbonmonoxy forms of chain-specific, isotopically (^{15}N and ^{2}H) labeled tetrameric hemoglobin (Hb) using ^{15}N-relaxation parameters [longitudinal relaxation rate (R_1), transverse relaxation rate (R_2), and heteronuclear nuclear Overhauser effect (NOE)] measured at two temperatures (29 and 34 °C) and two magnetic field strengths (11.7 and 14.1 T). In both deoxy and carbonmonoxy forms of human normal adult hemoglobin (Hb A), the amide N−H bonds of most amino acid residues are rigid on the fast time scale (nanosecond to picosecond), except for the loop regions and certain helix−helix connections. Although rigid in deoxy-Hb A, β146His has been found to be free from restriction of its backbone motions in the CO form, presumably due to the rupture of its hydrogen bond/salt bridge network. We now have direct dynamics evidence for this structural transition of Hb in solution. While remarkably flexible in the deoxy state, α31Arg and β123Thr, neighbors in the intradimer ($\alpha_1\beta_1$) interface, exhibit stiffening upon CO binding. These findings imply a role for α31Arg and β123Thr in the intradimer communication but contradict the results from X-ray crystallography. We have also found that there is considerable flexibility in the intradimer ($\alpha_1\beta_1$) interface (i.e., B, G, and H helices and the GH corner) and possible involvement of several amino acid residues (e.g., α31Arg, β3Leu, β41Phe, β123Thr, and β146His) in the allosteric pathway. Several amino acid residues at the intradimer interfaces, such as β109Val, appear to be involved in possible conformational exchange processes. The dynamic picture derived from the present study provides new insights into the traditional description of the stereochemical mechanism for the cooperative oxygenation of Hb A based on X-ray crystallographic results.

Hemoglobin is an indispensable protein of vertebrates and is the classic molecule for understanding the structural basis of a complex set of cooperative, linked interactions. The oxygenation of hemoglobin is regulated by interactions between its O_2-binding sites (homotropic interactions) and interactions between individual amino acid residues in the protein molecule and various solutes (heterotropic interactions). Heterotropic effectors include hydrogen ions, chloride ions, CO_2, inorganic phosphate, inositol hexaphosphate (IHP),[1] and 2,3-bisphosphoglycerate (2,3-BPG). Human normal adult hemoglobin (Hb A) has a molecular mass of ∼64.5 kDa, consisting of four subunits, namely, two identical α-chains of 141 amino acids each and two identical β-chains of 146 amino acids each. For a review on hemoglobin, see Dickerson and Geis (*1*). The arrangement of the subunits (i.e., quaternary structure) of Hb depends on the ligation state of the protein. Two classical quaternary structures are the T (tense) form for the low-affinity deoxy-Hb and the R (relaxed) form for the high-affinity oxy-Hb (crystals grown in high salt conditions), first reported by Perutz (*2*). There are two distinct types of subunit interfaces, $\alpha_1\beta_1$ or $\alpha_2\beta_2$ (intradimer) and $\alpha_1\beta_2$ or $\alpha_2\beta_1$ (interdimer). On the basis of the crystal structures of ligated and unligated Hb A, the $\alpha_1\beta_2$ or $\alpha_2\beta_1$ interface undergoes a sliding motion in going from the deoxy to the oxy state, whereas the $\alpha_1\beta_1$ or $\alpha_2\beta_2$ interface remains unchanged during the ligation process. A new quaternary structure in the ligated state, R2 (crystals grown in low-salt conditions), was observed by Silva et al. (*3*), and more recently, the R2 structure has also been observed under high-salt conditions (*4*). Kavanaugh et al. (*5*) reported their crystallographic studies on a number of mutants with mutations in the β37Trp cluster and have identified structural transitions referred to as T-to-T_{high} quaternary transitions, i.e., between the quaternary T structure of wild-type deoxy-Hb A and an ensemble of related T-like quaternary structures that are induced by some mutations in the β37Trp cluster and/or by exposing crystals of wild-type or mutant deoxy-Hbs to O_2. Using residual dipolar coupling (RDC) measurements, we have found that the solution structure of HbCO A is a dynamic ensemble of R and R2 crystal structures (*6*).

† This work is supported by research grants from the National Institutes of Health (R01HL-024525 and S10RR-017815).

* Address correspondence to this author. Phone: 412-268-3395. Fax: 412-268-7083. E-mail: chienho@andrew.cmu.edu.

‡ Present address: Department of Chemistry, Simon Fraser University, Vancouver, Canada.

[1] Abbreviations: Hb A, human normal adult hemoglobin; HbCO, carbonmonoxyhemoglobin; deoxy-Hb, deoxyhemoglobin; met-Hb, methemoglobin; NMR, nuclear magnetic resonance; R_1, longitudinal relaxation rate; R_2, transverse relaxation rate; *S*, generalized order parameter; RDC, residual dipolar coupling; NOE, nuclear Overhauser effect; IHP, inositol hexaphosphate; 2,3-BPG, 2,3-bisphosphoglycerate; HSQC, heteronuclear single-quantum coherence; TROSY, transverse relaxation-optimized spectroscopy.

10.1021/bi602654u CCC: $37.00
Published on Web 05/12/2007

More recently, we have assigned the polypeptide backbone resonances of deoxy-Hb A (*7*) and have observed spontaneous preferential orientation of deoxy-Hb A in solution at high magnetic fields, thus allowing us to obtain RDC values (*8*). By comparing the measured RDCs with the calculated RDCs (based on the crystal structure of deoxy-Hb A, PDB ID 1XXT), it appears that the solution structure of deoxy-Hb A may also be different from the crystal structure. The functional properties of Hb A in crystals are distinctly different from those in solution (*9*). This raises a very important point, namely, whether the structure of Hb in solution is not the same as that in the crystalline state, or the crystal structure may be one of many possible structures that can exist in solution. Thus, the conformational states (e.g., motion of the polypeptide chains and/or side chains) of the Hb molecule in solution and in crystals could be different. In order to better understand the Hb molecule, we need to correlate its structure, dynamics, and function in deoxy, oxy, and partially oxygenated states under physiological conditions. The CO-ligated form of Hb A is a good model for the oxy form and is considerably more stable, thus being more amenable for time-consuming NMR measurements than the oxy form that oxidizes spontaneously over time in solution becoming the nonfunctional methemoglobin (met-Hb).

The development of high-field multinuclear, multidimensional NMR and isotopic labeling techniques offers a realistic possibility for determining the structures of proteins of the size of Hb A and their dynamic properties in solution (*6*, *8*, *10*−*20*). This opens up the possibility of making a direct comparison between the crystal and solution structures of Hb A and of correlating the information derived from kinetic, thermodynamic, and spectroscopic studies with that obtained from studies of structure. Many of the controversial issues discussed above may then be resolved.

In this paper, we describe our results on the polypeptide backbone dynamics of Hb A in both deoxy and CO forms based on the Model-free analysis (*21*, *22*) as a first step to correlate the structure, dynamics, and function relationship of this important allosteric protein. We have found some interesting results, and some of them are not predicted by crystal structures of Hb A in deoxy and CO forms. For example, we have found that there is considerable flexibility in the intradimer ($\alpha_1\beta_1$ or $\alpha_2\beta_2$) interface (i.e., B, G, and H helices and the GH corner) and possible involvement of several amino acid residues (e.g., α31Arg, β3Leu, β41Phe, β123Thr, and β146His) in the allosteric pathway. Two residues, α31Arg and its neighbor, β123Thr, exhibit interesting dynamic behavior and suggest that they play a role as cementing and communicating connectors between the two intradimer ($\alpha_1\beta_1$ and $\alpha_2\beta_2$) subunits.

MATERIALS AND METHODS

Hb A Samples. Uniformly (^{2}H,^{15}N) labeled recombinant Hb A was expressed and purified as described previously (*23*, *24*). Two types of chain-specifically labeled hemoglobin samples, namely, (α-labeled)(β-unlabeled) and (α-unlabeled)-(β-labeled), each in the deoxy or CO form, were prepared by the procedures used in our laboratory (*12*, *25*), equilibrated with 0.1 M sodium phosphate buffer at pH 7.0 in 90% water and 10% D_2O, reaching a final Hb concentration of 5% (∼0.8 mM). These α- and β-chain chain-specifically labeled tetrameric Hb samples were used in all of our relaxation measurements.

^{15}N Relaxation Measurements. The backbone ^{15}N R_1, R_2, and steady-state ^{15}N−{^{1}H} NOE were measured at 11.7 and 14.1 T on Bruker DRX-500 and DRX-600 NMR spectrometers at 29 and 34 °C using 5 mm inverse detection probes equipped with triple-axis pulsed-field gradients. The pulse sequences of Farrow et al. (*26*, *27*) were used with minor modifications. The carrier frequency for the directly detected ^{1}H dimension was set to the water resonance, with spectral widths of 20.0 ppm for the deoxy samples and 17 ppm for the CO samples at both fields, using digital quadrature (DQD) detection and typical time domain of 2K (1024 complex points). The water signal was suppressed using the 3-9-19 WATERGATE sequence. For the indirectly detected (^{15}N) dimension, the spectral width was typically 25 ppm for the CO samples and 20.6 or 22.8 ppm for deoxy, with the carrier at 122 ppm (CO) and at 121 or 118 ppm for deoxy. Typically, 128 time domain points (64 complex) were acquired in the States mode (with receiver phase inversion). ^{15}N R_1 relaxation rates were measured using eight data points with seven relaxation delays (repeated values marked with *): 0.11, 0.33, 0.66, 1.32*, 2.64, 4.4, and 6.6 s for both fields.^{15}N R_2 experiments were performed with 8-relaxation delays (10 data points): 0, 16, 32*, 48, 64*, 80, 96, and 112 ms for both fields. Both R_1 and R_2 measurements were performed with a 3 s recovery delay and typically 32 (at 14.1 T) or 48 scans (at 11.7 T). Heteronuclear NOE measurements were performed using similar spectral parameters, except that for the ^{15}N dimension sometimes the time domain was 96, other times up to 140. Typically, the number of scans was 96, but up to 144 were used on occasion. The NOE experiment employed a 12 s proton saturation period, and the control (no NOE) employed a 12 s delay instead. NMR relaxation data were processed using NMRPipe (*28*) software on SGI or SUN workstations. The peak heights and volumes of the cross-peaks were calculated using the nonlinear least-squares fit (nlinLS) implemented in NMRPipe.

Analysis of Relaxation Data. The backbone dynamics information of Hb was obtained on the basis of the Model-free formalism, as described by Lipari, Szabo, Clore, and co-workers (*21*, *22*, *29*). The order parameter (simplified term of the square of the generalized order parameter), S^2, describes the amplitude of the internal picosecond to nanosecond motions of a particular bond vector and ranges from $S^2 = 0$ for a bond vector rapidly and isotropically sampling multiple orientations to $S^2 = 1$ for no internal motion. The order parameter S^2 can be fitted by an "extended model" from the NMR spectral density functions at the Larmor frequencies ω for certain spins (^{1}H, ^{15}N, ^{13}C, etc.), $J(\omega)$, as

$$J(\omega) = \frac{2}{5}\left[\frac{S^2\tau_m}{1+(\omega\tau_m)^2} + \frac{(1-S_f^2)\tau'_f}{1+(\omega\tau'_f)^2} + \frac{(S_f^2-S^2)\tau'_s}{1+(\omega\tau'_s)^2}\right] \quad (1)$$

where $\tau'_f = \tau_f\tau_m/(\tau_f + \tau_m)$, $\tau'_s = \tau_s\tau_m/(\tau_s + \tau_m)$, with τ_m as the isotropic rotational correlation time of the molecule, τ_f and τ_s as the effective correlation times for internal motions on a fast time scale (τ_f < 100−200 ps) and slow time scale

Table 1: Isotropic, Axially Symmetric, and Fully Anisotropic Diffusion Parameters Determined for Deoxy and CO (in Parentheses) Forms of Hb Using R1R2_Diffusion(I) and Quadric_1.11(II)[a]

deoxy (CO)		tensor	field (T)	$\tau_{c,eff} = (6D_{iso})^{-1}$ (ns)	$2D_z/(D_x + D_y)$	D_x/D_y
29 °C	I	isotropic	11.7	32.74 ± 0.05 (32.00 ± 0.06)		
			14.1	31.62 ± 0.05 (30.68 ± 0.06)		
		axial	11.7	32.71 ± 0.05 (32.07 ± 0.06)	1.09 ± 0.01 (1.07 ± 0.01)	
			14.1	31.65 ± 0.05 (30.75 ± 0.06)	1.12 ± 0.01 (1.11 ± 0.02)	
	II	isotropic	11.7	32.93 ± 0.05 (32.06 ± 0.06)		
			14.1	31.92 ± 0.05 (30.79 ± 0.06)		
		axial	11.7	32.98 ± 0.05 (32.13 ± 0.06)	1.10 ± 0.01 (1.08 ± 0.01)	
			14.1	31.89 ± 0.05 (30.84 ± 0.06)	1.11 ± 0.01 (1.13 ± 0.02)	
		anisotropic	11.7	32.91 ± 0.06 (32.15 ± 0.07)	1.09 ± 0.01 (1.07 ± 0.01)	1.06 ± 0.01 (1.04 ± 0.01)
			14.1	31.94 ± 0.06 (30.80 ± 0.06)	1.11 ± 0.01 (1.14 ± 0.02)	1.05 ± 0.01 (1.04 ± 0.02)
34 °C	I	isotropic	11.7	28.90 ± 0.03 (27.91 ± 0.05)		
			14.1	28.04 ± 0.03 (27.58 ± 0.04)		
		axial	11.7	28.80 ± 0.03 (28.02 ± 0.05)	1.10 ± 0.01 (1.05 ± 0.01)	
			14.1	28.08 ± 0.04 (27.69 ± 0.04)	1.11 ± 0.01 (1.06 ± 0.01)	
	II	isotropic	11.7	29.05 ± 0.04 (27.96 ± 0.05)		
			14.1	28.27 ± 0.04 (27.63 ± 0.04)		
		axial	11.7	28.94 ± 0.03 (27.98 ± 0.05)	1.10 ± 0.01 (1.06 ± 0.01)	
			14.1	28.28 ± 0.04 (27.70 ± 0.04)	1.12 ± 0.01 (1.10 ± 0.01)	
		anisotropic	11.7	28.94 ± 0.04 (28.05 ± 0.06)	1.10 ± 0.01 (1.05 ± 0.01)	1.01 ± 0.01 (1.04 ± 0.01)
			14.1	28.27 ± 0.04 (27.71 ± 0.05)	1.12 ± 0.01 (1.09 ± 0.01)	1.01 ± 0.01 (1.01 ± 0.01)

[a] Principal components only.

($\tau_f < \tau_s < \tau_m$), respectively, $S^2 = S_f^2 S_s^2$ is the square of the generalized order parameter, and S_f^2 and S_s^2 are the squares of the order parameters for the internal motions on the fast and slow time scales. The spectral density functions are computed from the experimental relaxation parameters, R_1, R_2, and NOE, by (*30*)

$$R_1 = (d^2/4)[J(\omega_H - \omega_X) + 3J(\omega_X) + 6J(\omega_H + \omega_X)] + c^2 J(\omega_X)$$

$$R_2 = (d^2/8)[4J(0) + J(\omega_H - \omega_X) + 3J(\omega_X) + 6J(\omega_H) + 6J(\omega_H + \omega_X)] + (c^2/6)[4J(0) + 3J(\omega_X)] + R_{ex}$$

$$\mathrm{NOE} = 1 + (d^2/4R_1)(\gamma_H/\gamma_X)[6J(\omega_H + \omega_X) - J(\omega_H - \omega_X)] \quad (2)$$

where $d = \mu_0 h \gamma_X \gamma_H \langle r_{XH}^{-3} \rangle / (8\pi^2)$, $c = \omega_X \Delta\sigma/(3)^{1/2}$, μ_0 is the permeability of free space, h is Planck's constant, γ_H and γ_X are the gyromagnetic ratios of ^{1}H and the X spin (X = ^{13}C or ^{15}N), respectively, r_{XH} is the X−H bond length [r_{NH} = 1.02 Å (*31*) was used in our analysis], and $\Delta\sigma = \sigma_{||} - \sigma_\perp$ is the chemical shift anisotropy in an axial symmetric system of the X spin [$\Delta\sigma = -172$ ppm (*32*) was used for ^{15}N in our analysis].

The Model-free program version 4.10 (*33*) was used in our backbone dynamics analysis. This program uses Monte Carlo simulations to estimate uncertainties in the Model-free parameters and helps to assign appropriate models for different residues according to a statistical protocol including the *F*-test (*33*, *34*). Five subsets of the above extended model are provided for model selection, with reduced number of parameters under certain conditions (as in the parentheses): (1) $S^2 = S_f^2$, ($S_s^2 = 1$, $\tau_f \rightarrow 0$, $\tau_s = 0$); (2) $S^2 = S_f^2$, $\tau_e = \tau_f$, ($S_s^2 = 1$, $\tau_s = 0$); (3) $S^2 = S_f^2$, R_{ex}, ($S_s^2 = 1$, $\tau_f = 0$, $\tau_s = 0$); (4) $S^2 = S_f^2$, $\tau_e = \tau_f$, R_{ex}, ($S_s^2 = 1$, $\tau_s = 0$); (5) S_f^2, S^2, $\tau_e = \tau_s$, ($\tau_f \rightarrow 0$). In the models with R_{ex}, nonzero chemical exchange contributions to the R_2 relaxation rates are considered.

We have applied the statistical approach, as described by Mandel et al. (*33*), to assign the best motional model for each amino acid residue. Most residues can be fitted satisfactorily. For each residue not fitted well by any of the five models, the model with the minimum sum of squared errors (SSE) between the dynamic model and the experimental data was used (*35*).

A complete listing of our relaxation data for deoxy- and carbonmonoxy-Hb A at 11.7 and 14.1 T and at 29 and 34 °C is given in Supporting Information.

Diffusion parameters were determined independently by two different programs, R2R1-Diffusion (*36*) and Quadric_diffusion 1.11 (*37*). Three-dimensional crystal structures of Hb A [PDB IDs 1A3N (*38*) and 1BBB (*3*)] were used for deoxy- and carbonmonoxy-Hb A, respectively. All residues with NOE <0.65 and significantly deviating R_2/R_1 and R_1R_2 values (*39*) were excluded from the analysis.

RESULTS

Uniformly (^{2}H,^{15}N) chain-specifically labeled deoxy- and carbonmonoxy-Hb A samples were prepared as 5% solutions (~0.8 mM) in aqueous phosphate buffer. The polypeptide backbone ^{15}N R_1, R_2, and steady-state ^{15}N−{^{1}H} NOE were measured at 11.7 and 14.1 T at 29 and 34 °C. The backbone dynamics information of Hb A was obtained on the basis of the Model-free formalism. S^2, the square of the generalized order parameter, describes the amplitude of internal picosecond to nanosecond motions for a particular bond vector and ranges from $S^2 = 0$, for a bond vector rapidly sampling multiple orientations, to $S^2 = 1$, for no internal motion. Diffusion parameters τ_c, $2D_z/(D_x + D_y)$, and D_x/D_y were determined independently by two different programs, R2R1-Diffusion (*36*) and Quadric_diffusion 1.11 (*37*) (see Materials and Methods for details).

Diffusion Analysis. The principal components of the diffusion tensors are summarized in Table 1. The values of the relaxation parameters, $\tau_c = (6D_{iso})^{-1}$, $2D_z/(D_x + D_y)$, and D_x/D_y, obtained from different methods, are essentially identical. There is an apparent and expected temperature

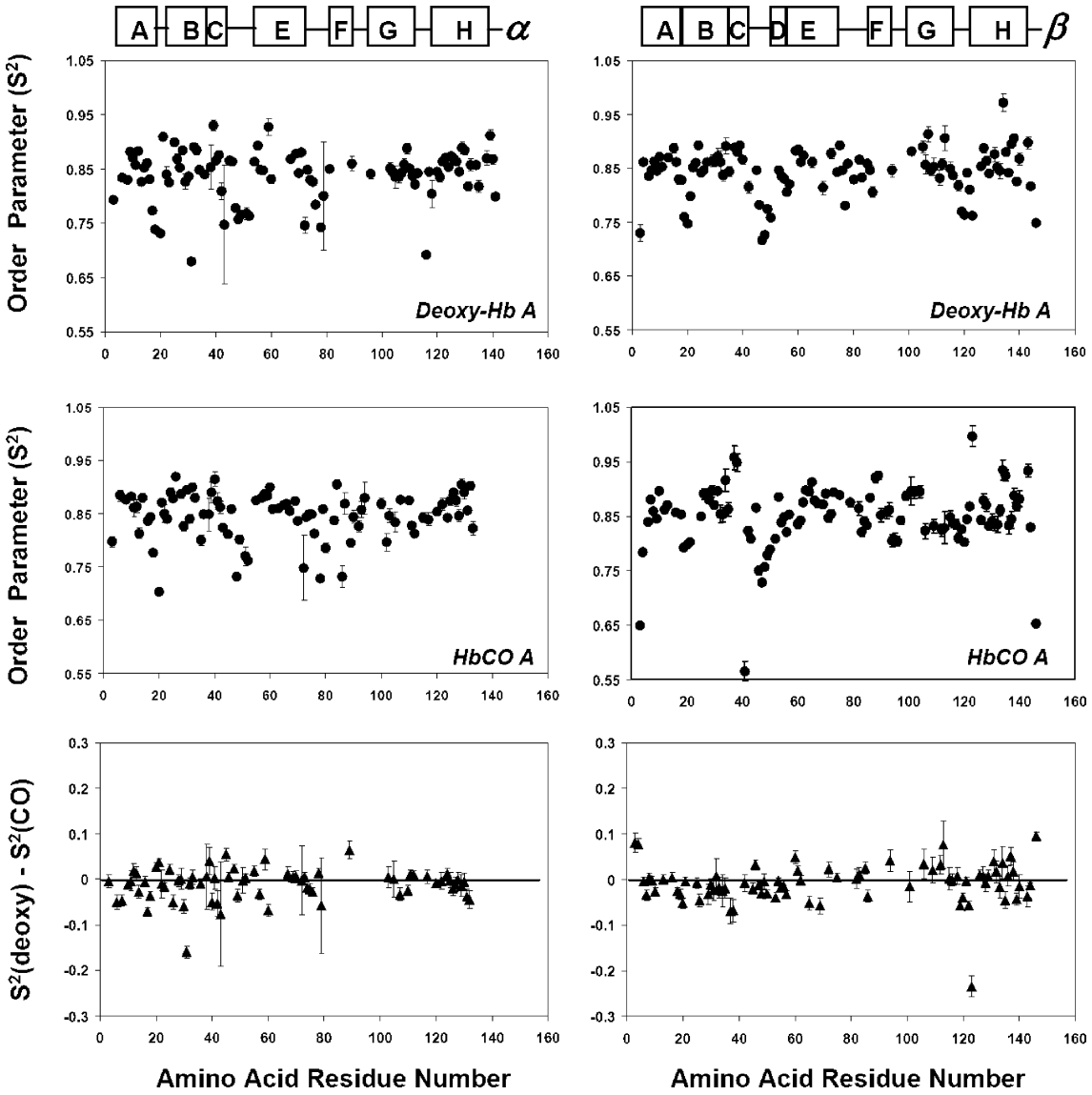

FIGURE 1: Order parameters (S^2) of amide N−H bonds in Hb at 29 °C.

effect on the tumbling time, τ_c, with shorter τ_c at 34 °C (27.5−29 ns) than that at 29 °C (31.5−33 ns). Slightly but uniformly, under the same conditions, τ_c values for HbCO A are shorter than those for deoxy-Hb A; also slightly but uniformly, for the same sample, τ_c values measured at the higher field (14.1 T) are shorter than those at the lower field (11.7 T), when other experimental conditions are identical. The anisotropy ratios, $2D_z/(D_x + D_y)$, are around 1.10, showing slight rotational anisotropy of Hb, with no significant variation for different forms and conditions.

Model-Free Analysis. As seen in Figure 1, deoxy-Hb A and HbCO A share similar backbone mobility distribution profiles, where the amide N−H bonds of most amino acid residues are rigid, except for the loop regions. The CE loop (F43−G51), EF loop (H72−A79), and GH loop (L113−F117) in the α-chain and the CD loop (E43−S49), EF loop (H77−T84), and GH loop (F118−F122) in the β-chain are apparently more mobile than the neighboring helical regions. There is no loop structure between the A and B helices. However, the residues close to the A−B connection, V17−G22 in the α-chain and V18−D21 in the β-chain, exhibit great flexibility, comparable to any of the loop regions. On the other hand, some residues, such as T39 and G59 in the α-chain and F37, T38, V134, and A135 in the β-chain, are consistently very rigid in all cases.

Besides the common helix−loop contrast in both the deoxy and carbonmonoxy forms of Hb A, certain amino acid residues demonstrate differential rigidity with and without CO binding (Figure 1). Two neighboring residues at the intradimer ($\alpha_1\beta_1$ or $\alpha_2\beta_2$) interface, α31Arg and β123Thr, exhibit the most dramatic mobility change due to CO binding, with greatly increased rigidity in the carbonmonoxy form, compared to that in the deoxy form, at both 29 and 34 °C. To a lesser degree, the motion at residue β69Gly is also more restricted in HbCO A. On the contrary, residues β146His and β3Leu (not shown in Figure 1 but shown in Supporting Information) become more flexible in the CO form than in the deoxy form. β41Phe is among the most mobile residues in HbCO A. Unfortunately, no comparable dynamics information for β41Phe is available for the deoxy form, as this residue does not give rise to an observable signal.

According to the Model-free formalism, the R_{ex} terms in models 3 and 4 are indicators of slow (microsecond to millisecond time scale) conformational exchange processes.

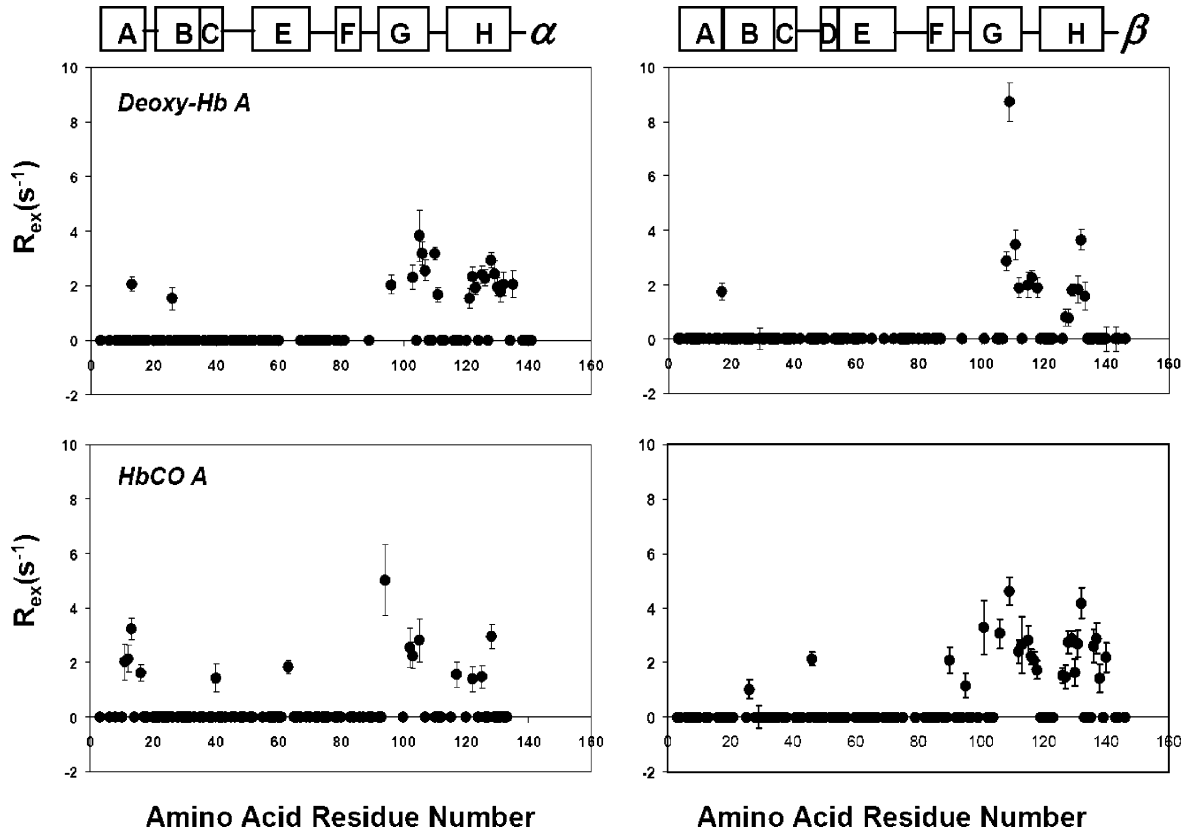

FIGURE 2: R_{ex} terms from Model-free analysis for deoxy-Hb A and HbCO A at 34 °C. Possible chemical exchange processes are implied at amino acid residues after 100, including the most dramatic β109Val.

We report the R_{ex} terms obtained for our Hb samples in Figure 2. In both deoxy- and CO-ligated states, β109Val has very high R_{ex} values at both 29 and 34 °C, but the magnitudes of R_{ex} terms for this residue are significantly modified after CO binding. The amino acid residues after 100, close to the C-terminus, apparently need R_{ex} terms in fitting more than do other parts of the protein molecule, implying possible slow time scale dynamic events at the GH corners and H helices of both chains. These regions are not at the interdimer ($\alpha_1\beta_2$ or $\alpha_2\beta_1$) interfaces but instead at the intradimer ($\alpha_1\beta_1$ or $\alpha_2\beta_2$) interfaces, which were previously considered a rigidly packed region in the Hb structure.

DISCUSSION

Mobility Change of β146His and the Interdimer "Switch" Region. As discussed above, the backbone order parameter S^2 reflects the degree of mobility of the amide N−H bond. For example, as the C-terminal residue, β146His displays high rigidity in deoxy-Hb A, with order parameter values comparable to the helical parts of the protein (Figure 1). The restricted mobility of β146His can be explained because in the T state of Hb, β146His is involved in two strong interactions with neighboring residues, e.g., a salt bridge to α40Lys and an H-bond to β94Asp (*1*, *40*). β146His is a key residue in the so-called switch region at the interdimer ($\alpha_1\beta_2$ or $\alpha_2\beta_1$) interfaces. As one of the important events during the allosteric transition of Hb from the T to R state, a dimer−dimer rotation unlocks β146His from both salt bridge and H-bond interactions with its neighbors (*1*). As a consequence, the order parameter (S^2) of β146His amide N−H becomes as low as that seen for a loop region. This is the first dynamic evidence to support the removal of interaction at the C-terminus (β145Tyr, β146His, etc.) of the β-chain during the cooperative oxygenation process of Hb A.

CO-Induced Stiffening of α31Arg and β123Thr at the Intradimer ($\alpha_1\beta_1$ or $\alpha_2\beta_2$) Interfaces. The intradimer ($\alpha_1\beta_1$ or $\alpha_2\beta_2$) interfaces can no longer be considered merely passive parts of the allosteric machinery of Hb, a result of recent experimental and computational evidence as to their roles in the allosteric signal transduction (*41*−*47*). Although the molecular dynamics simulation by Ramadas and Rifkin (*42*) implied that a frozen intradimer ($\alpha_1\beta_1$ or $\alpha_2\beta_2$) interface can block the heme−heme communication within the $\alpha\beta$ dimer, X-ray crystallography results indicate no flexibility in this so-called "subunit packing" region. Specifically, the "cementing" residue, α31Arg, according to X-ray crystallography is involved in a very stable interaction network with neighboring β122Phe and β127Gln. The triangle formed by these three residues, along with other subunit-crossing interactions involving β30Arg, α117Phe, and α122His, contributes to the tight G-H-B packing of the $\alpha_1\beta_1$ or $\alpha_2\beta_2$ dimer (*1*, *41*, *46*, *48*, *49*). In our present study, the order parameter values for the amide N−H bonds of α31Arg and one of its neighboring residues at the beginning of the β H helix, β123Thr, are consistently low in deoxy-Hb A at both 29 and 34 °C, showing great flexibility for these two residues. This observation implies that one of the two "clinching bolts" at the intradimer interfaces is loosened in the deoxy (T) state in solution. Interestingly, this finding contradicts the X-ray crystallography results for deoxy-Hb A. Then, according to the NMR dynamics data (Figure 1), this "loosened bolt" in the deoxy state is tightened after CO binding, as it demonstrates high rigidity in the ligated state.

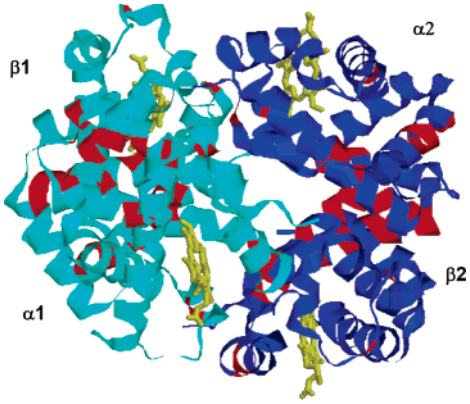

FIGURE 3: HbCO A at 34 °C with the amino acid residues with significant R_{ex} values colored red. Amino acid residues in the G and H helices of both α- and *β*-chains are possibly involved in chemical exchange processes.

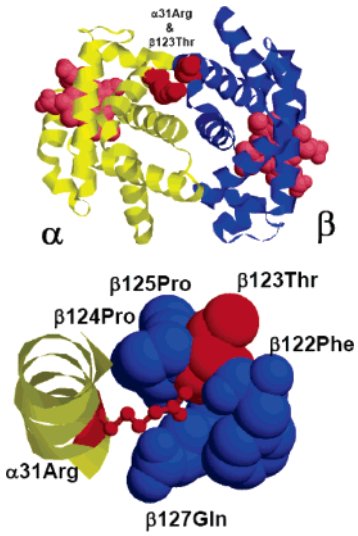

FIGURE 4: Residues α31Arg and *β*123Thr are shown at the intradimer ($\alpha_1\beta_1$ or $\alpha_2\beta_2$) interface of Hb A. The amide N−H bonds of these two amino acid residues exhibit unusual flexibility in deoxy-Hb A, but both become rigid in HbCO A.

A high-resolution crystal structure of deoxy-Hb A (PDB ID 1A3N) (*38*) shows a tightly packed "hot-dog" picture of the α31Arg side-chain arm and a groove in the *β*-subunit formed by *β*122Phe, *β*123Thr, *β*124Pro, *β*125Pro, and *β*127Gln (Figure 4). There is an H-bond between α31Arg and *β*122Phe and an H-bond between α31Arg and *β*127Gln, according to X-ray crystallography. From our result, the unusual mobility of this region occurs at where α31Arg contacts *β*123Thr and two prolines (*β*124Pro and *β*125Pro). The flexibility of α31Arg and *β*123Thr is possibly due to the motion of the *β*-H helix at its beginning end, where the proline twins are located. An alternative explanation is the absence of H-bonds involving α31Arg in the solution, as it is possible that the solid packing in the crystal form sometimes can generate extra close contacts between amino acid residues, simulating an H-bond. No matter what actually contributes to the mobility contrast in this region before and after ligand (CO) binding, this observation implies that certain signal transduction or energy distribution crosses the intradimer interface during the allosteric transition of Hb.

On the contrary, as an element in another "cementing unit" of the intradimer assembly, *β*30Arg shows consistently high backbone rigidity in both deoxy and CO forms. However, α122His, a member of this second intradimer triangle locking region, along with α103His, has been found to be structurally more stabilized in the R state than the T state by solvent exchange methods, implying a dynamic variation of certain degree, though less significant than in the α31Arg−*β*123Thr case (*50*, *51*). For this second triangle network, as for the first one involving α31Arg and *β*123Thr, X-ray crystallography gives no evidence of the removal of surrounding interactions (H-bond or salt bridges) of α122His in the T state (*48*). α31Arg and *β*30Arg are at the far ends of the distal heme pockets of the α-chain and *β*-chain, respectively. As previously mentioned, the distal pockets of α- and *β*-chains are found to be not identical in many aspects, including their ligand accessibility, cavity size in the T state, and the strengths of their H-bonds to the ligands in the R states (*2*, *25*, *45*, *52*). The loose−rigid switch of the α31Arg−*β*123Thr region during the T−R transition suggests that the ligand binding at the α-subunit might induce a tightening lock of the same dimer α- and *β*-subunits at the α31Arg−*β*123Thr site, thus initiating intradimer signal transduction from the distal side of the α-heme pocket. This observation provides support to the intradimer sequential cooperativity during Hb allostery.

Comparison of S^2 Values with Crystallographic B-Factors. In the present study, we have observed no apparent correlation between the amide N−H order parameters and the *B*-factors for backbone nitrogen atoms, except that a minor inverse correlation is seen in the N- and C-terminal residues as well as some of the loops connecting helices. As has been suggested (*33*), the varying degrees of inverse correlation between S^2 values and *B*-factors arise mainly from the insensitivity of the order parameters to translational displacements. In fact, since the frequency of Larmor precession of nuclei matches only the frequencies of rotational motions, the faster processes including bond vibrations do not affect the order parameter. A plot comparing the crystallographic *B*-factors of Hb A and the NMR order parameters obtained at 29 °C can be found in Figure 3S (Supporting Information).

Mobility Change at the α-C Terminus upon CO Binding. Amino acid residues after 138 at the C-terminus of the α-chain in HbCO A are not visible in the HSQC and TROSY spectra (*53*). These α-C-terminal residues, however, have normal peak intensities in the spectra of deoxy-Hb A and demonstrate high rigidity for α139Lys and α140Tyr, according to Model-free analysis (Figure 1). The α-C terminus of Hb is near the so-called "flexible joint" area at the interdimer interface and is surrounded by several H-bonds and salt bridges in deoxy-Hb A (*1*). The disappearance of the NMR signals of these residues in the CO form might be due to their flexible state, a consequence of the breaking of the H-bonds and salt bridges during the T → R allosteric transition (*1*). Such an interpretation is supported by the *B*-factor plot, as shown in Supporting Information, depicting a sharp increase of the *B*-factor for residues past 138 (Figure 3S).

Conformational Exchange at G and H Helices Implied by R_{ex} Terms. A nonzero R_{ex} term obtained from Model-free analysis is not solid evidence for the conformational exchange process. However, the significantly large R_{ex} values of certain residues, such as *β*109Val, and the frequent occurrence of nonzero R_{ex} terms among the amino acid residues after 100 imply a high likelihood of slow time scale

(microsecond to millisecond) motions in the G and H helices. Interestingly, these residues are not at the FG corner or C helices where the interdimer hinge areas (so-called "joint" and "switch" regions) are located, but are along the intradimer ($\alpha_1\beta_1$ and $\alpha_2\beta_2$) interfaces (Figures 2 and 3). This observation is not sufficient to exclude the existence of certain types of conformational flexibility at the joint and switch regions, but obviously these motions are invisible to the R_{ex} indicators. Questions thus arise about whether the mobility of the amino acid residues at the interdimer hinge regions could be affected by the sliding movement between the two dimers. This sliding movement was considered as the major conformational change during the T → R → R2 quaternary transition (*54*). The time scale of this dimer−dimer sliding and the relative populations of the three or more sliding intermediate states are the two key factors for the feasibility of using NMR methods to detect this dynamic event.

Rigidity Fluctuations between Deoxy- and Carbonmonoxy-Hb A. Our results show that the order parameters (S^2) of the backbone N−H bonds of Hb A do not have a uniform trend of variation upon CO binding but fluctuate slightly within a range of 0.1, different from residue to residue (Figure 1). Since the work of Lipari and Szabo (*22*), the amplitude of order parameters has been correlated to the thermodynamic properties, entropy in particular, of proteins (*55*−*57*). However, the trend of the variation of backbone or side-chain rigidity, in response to ligand binding, could be either increasing (*57*−*59*) or decreasing (*15*, *60*−*62*). The backbone disordering discussed above is not the sole contribution to the entropy of a protein system. Mobility of protein side chains (*57*, *63*), motions, and conformational variations on time scales other than nanosecond to picosecond, as well as solvent factors, could also affect the general entropy level. Adding to this complexity, the paramagnetic environment at the heme sites could also alter the relaxation properties of the spin systems, leading to extra errors in the entropy estimation.

Finally, we need to emphasize that in the above discussions about the mobility of Hb amino acid residues, we mean the motion of the protein backbone, as characterized by the amide N−H bonds. This is, in fact, a convenient simplification. The side chains of the amino acid residues can act very differently in their dynamic behaviors, with much lower barriers for their motions, compared to structurally more constrained polypeptide backbones (*64*). Thus, biological processes that do not affect the rigidity of protein backbone scaffold may still significantly perturb the side-chain motions (*57*). To achieve a complete correlation between dynamics and Hb functions, a thorough investigation of side-chain dynamics of Hb is necessary.

In conclusion, our present NMR studies of the polypeptide backbone dynamics of Hb A in both deoxy and carbonmonoxy forms have provided new information regarding the structural and dynamic properties of this protein not available from the traditional crystal structures. There are clear differences in the backbone dynamics between the deoxy and carbonmonoxy forms in several regions of the Hb molecule, especially in the intra- and interdimer interfaces. For example, α31Arg and β123Thr located in the intradimer interface are flexible in the deoxy state, but exhibit stiffening upon ligation of the Hb molecule. These two residues exhibit interesting dynamic behavior and may suggest that they can play a role as cementing and communicating connectors between the two intradimer ($\alpha_1\beta_1$ and $\alpha_2\beta_2$) interfaces. β146His, a key residue in the allostery of the Hb molecule, becomes flexible upon ligation. Thus, further structural and dynamic studies of Hb A in solution in conjunction with appropriate functional studies will help elucidate the structural, dynamic, and functional basis for the allostery of this interesting protein molecule at atomic resolution.

ACKNOWLEDGMENT

We thank Dr. Qingguo Gong and Dr. David H. Maillet for helpful discussions. We also thank Dr. Arthur G. Palmer for providing the Model-free 4.10 program used in this work.

SUPPORTING INFORMATION AVAILABLE

Figure 1S, order parameters (S^2) of amide N−H bonds in Hb at 34 °C; Figure 2S, R_{ex} terms derived from Model-free analysis for deoxy-Hb A and HbCO A at 29 °C; Figure 3S, X-ray crystallographic *B*-factors (filled circles) and NMR order parameters (open circles, obtained at 29 °C) [top, deoxy-Hb A, with *B*-factors from 1A3N (PDB ID); bottom, HbCO A, with *B*-factors from 1BBB (PDB ID)]; Figure 4S, NMR relaxation parameters of backbone amide ^{15}N in Hb A at 29 °C (filled circles) and 34 °C (open circles) [conditions: (1) deoxy-Hb A at 11.7 T; (2) deoxy-Hb A at 14.1 T; (3) HbCO A at 11.7 T; (4) HbCO A at 14.1 T]; Figure 5S, R_1 and R_2 relaxation decay curves for amide ^{15}N in two amino acid residues (α31Arg and β146His) at 29 °C (repeated data points are indicated by arrows); Table 1S, NMR relaxation parameters of backbone amide ^{15}N in deoxy-Hb A; Table 2S, NMR relaxation parameters of backbone amide ^{15}N in HbCO A; Table 3S, amino acid residues in Hb A selected for correlation time determination. This material is available free of charge via the Internet at http://pubs.acs.org.

REFERENCES

1. Dickerson, R. E., and Geis, I. (1983) *Hemoglobin: structure, function, evolution, and pathology*, Benjamin-Cummings, Menlo Park, CA.
2. Perutz, M. F. (1970) Stereochemistry of cooperative effects in haemoglobin, *Nature 228*, 726−739.
3. Silva, M. M., Rogers, P. H., and Arnone, A. (1992) A third quaternary structure of human hemoglobin A at 17 Å resolution, *J. Biol. Chem. 267*, 17248−17256.
4. Safo, M. K., and Abraham, D. J. (2005) The enigma of the liganded hemoglobin end state: a novel quaternary structure of human carbonmonoxy hemoglobin, *Biochemistry 44*, 8347−8359.
5. Kavanaugh, J. S., Rogers, P. H., and Arnone, A. (2005) Crystallographic evidence for a new ensemble of ligand-induced allosteric transitions in hemoglobin: the T-to-T_{high} quaternary transitions, *Biochemistry 44*, 6101−6121.
6. Lukin, J. A., Kontaxis, G., Simplaceanu, V., Yuan, Y., Bax, A., and Ho, C. (2003) Quaternary structure of hemoglobin in solution, *Proc. Natl. Acad. Sci. U.S.A. 100*, 517−520.
7. Sahu, S. C., Simplaceanu, V., Ho, N. T., Giovannelli, J. L., and Ho, C. (2006) Backbone resonance assignment of human adult hemoglobin in the deoxy form, *J. Biomol. NMR 36*, 1.
8. Sahu, S. C., Simplaceanu, V., Gong, Q., Ho, N. T., Glushka, J. G., Prestegard, J. H., and Ho, C. (2006) Orientation of deoxyhemoglobin at high magnetic fields: structural insights from RDCs in solution, *J. Am. Chem. Soc. 128*, 6290−6291.
9. Eaton, W. A., Henry, E. R., Hofrichter, J., and Mozzarelli, A. (1999) Is cooperative oxygen binding by hemoglobin really understood, *Nat. Struct. Biol. 6*, 351−358.

10. Wüthrich, K. (2003) NMR studies of structure and function of biological macromolecules (Nobel Lecture), *Angew. Chem., Int. Ed. 42*, 3340−3363.
11. Gardner, K. H., and Kay, L. E. (1998) The use of ^{2}H, ^{13}C, ^{15}N multidimensional NMR to study the structure and dynamics of proteins, *Annu. Rev. Biophys. Biomol. Struct. 27*, 357−406.
12. Simplaceanu, V., Lukin, J. A., Fang, T.-Y., Zou, M., Ho, N. T., and Ho, C. (2000) Chain-selective isotopic labeling for NMR studies of large multimeric proteins: application to hemoglobin, *Biophys. J. 79*, 1146−1154.
13. Yuan, Y., Simplaceanu, V., Lukin, J. A., and Ho, C. (2002) NMR investigation of the dynamics of tryptophan side-chains in hemoglobins, *J. Mol. Biol. 321*, 863−878.
14. Kern, D., and Zuiderweg, E. R. (2003) The role of dynamics in allosteric regulation, *Curr. Opin. Struct. Biol. 13*, 748−757.
15. Palmer, A. G., III (2004) NMR characterization of the dynamics of biomacromolecules, *Chem. Rev. 104*, 3623−3640.
16. Gong, Q., Simplaceanu, V., Lukin, J. A., Giovannelli, J. L., Ho, N. T., and Ho, C. (2006) Quaternary structure of carbonmonoxy-hemoglobins in solution: structural changes induced by the allosteric effector inositol hexaphosphate, *Biochemistry 45*, 5140−5148.
17. Pervushin, K., Riek, R., Wider, G., and Wuthrich, K. (1997) Attenuated T_2 relaxation by mutual cancellation of dipole-dipole coupling and chemical shift anisotropy indicates an avenue to NMR structures of very large biological macromolecules in solution, *Proc. Natl. Acad. Sci. U.S.A. 94*, 12366−12371.
18. Sui, X., Xu, Y., Giovannelli, J. L., Ho, N. T., Ho, C., and Yang, D. (2005) Mapping protein-protein interfaces on the basis of proton density difference, *Angew. Chem., Int. Ed. 44*, 5141−5144.
19. Wider, G., and Wüthrich, K. (1999) NMR spectroscopy of large molecules and multimolecular assemblies in solution, *Curr. Opin. Struct. Biol. 9*, 594−601.
20. Yang, D. W., Zheng, Y., Liu, D. J., and Wyss, D. F. (2004) Sequence-specific assignments of methyl groups in high-molecular weight proteins, *J. Am. Chem. Soc. 126*, 3710−3711.
21. Lipari, G., and Szabo, A. (1982) Model-free approach to the interpretation of nuclear magnetic resonance relaxation in macromolecules. 1. Theory and range of validity, *J. Am. Chem. Soc. 104*, 4546−4559.
22. Lipari, G., and Szabo, A. (1982) Model-free approach to the interpretation of nuclear magnetic resonance relaxation in macromolecules. 2. Analysis of experimental results, *J. Am. Chem. Soc. 104*, 4559−4570.
23. Shen, T.-J., Ho, N. T., Simplaceanu, V., Zou, M., Green, B. N., Tam, M. F., and Ho, C. (1993) Production of unmodified human adult hemoglobin in *Escherichia coli*, *Proc. Natl. Acad. Sci. U.S.A. 90*, 1085−1097.
24. Shen, T.-J., Ho, N. T., Zou, M., Sun, D. P., Cottam, P. F., Simplaceanu, V., Tam, M. F., Bell, D. A. J., and Ho, C. (1997) Production of human normal adult and fetal hemoglobins in *Escherichia coli*, *Protein Eng. 10*, 1085−1097.
25. Lukin, J. A., Simplaceanu, V., Zou, M., Ho, N. T., and Ho, C. (2000) NMR reveals hydrogen bonds between oxygen and distal histidines in oxyhemoglobin, *Proc. Natl. Acad. Sci. U.S.A. 97*, 10354−10358.
26. Farrow, N. A., Zhang, O., Forman-Kay, J. D., and Kay, L. E. (1995) Comparison of the backbone dynamics of a folded and an unfolded SH3 domain existing in equilibrium in aqueous buffer, *Biochemistry 34*, 868−878.
27. Grzesiek, S., and Bax, A. (1993) The importance of not saturating water in protein NMR. Application to sensitivity enhancement and NOE measurements, *J. Am. Chem. Soc. 115*, 12593−12594.
28. Delaglio, F., Grzesiek, S., Vuister, G., Zhu, G., Pfeiffer, J., and Bax, A. (1995) NMRPipe: a multidimensional spectral processing system based on UNIX pipes, *J. Biomol. NMR 6*, 277−293.
29. Clore, G. M., Szabo, A., Bax, A., Kay, L. E., Driscoll, P. C., and Gronenborn, A. M. (1990) Deviation from the simple two-parameter Model-free approach to the interpretation of nitrogen-15 nuclear magnetic relaxation of proteins, *J. Am. Chem. Soc. 112*, 4989−4991.
30. Abragam, A. (1961) *Principles of nuclear magnetism*, Clarendon Press, Oxford.
31. Jeffrey, G. (1992) Accurate molecular structures, their determination and importance, (Domenicano, A., and Hargittai, I., Eds.) pp 270−298, Oxford Science Publication, Oxford.
32. Kroenke, C. D., Rance, M., and Palmer, A. G., III (1999) Variability of the ^{15}N chemical shift anisotropy in *Escherichia coli* ribonuclease H in solution, *J. Am. Chem. Soc. 121*, 10119−10125.
33. Mandel, A. M., Akke, M., and Palmer, A. G., III (1995) Backbone dynamics of *Escherichia coli* ribonuclease HI: correlations with structure and function in an active enzyme, *J. Mol. Biol. 246*, 144−163.
34. Palmer, A. G., III, Rance, M., and Wright, P. E. (1991) Intramolecular motions of a zinc finger DNA-binding domain from Xfin characterized by proton-detected natural abundance ^{13}C heteronuclear NMR spectroscopy, *J. Am. Chem. Soc. 113*, 4371−4380.
35. Yao, S., Smith, D. K., Hinds, M. G., Zhang, J.-g., Nicola, N. A., and Norton, R. S. (2000) Backbone dynamics measurements on leukemia inhibitory factor, a rigid four-helical bundle cytokine, *Protein Sci. 9*, 671−682.
36. Tjandra, N., Feller, S. E., Pastor, R. W., and Bax, A. (1995) Rotational diffusion anisotropy of human ubiquitin from ^{15}N NMR relaxation, *J. Am. Chem. Soc. 117*, 12562−12566.
37. Lee, L. K., Rance, M., Chazin, W. J., and Palmer, A. G., III (1997) Rotational diffusion anisotropy of protein from simultaneous analysis of ^{15}N and ^{13}C nuclear spin relaxation, *J. Biomol. NMR 9*, 287−298.
38. Tame, J. R. H., and Vallone, B. (2000) The structures of deoxy human haemoglobin and the mutant Hb Tyra42His at 120K, *Acta Crystallogr., Sect. D: Biol. Crystallogr. 56* (Part 7), 805−811.
39. Kneller, J. M., Lu, M., and Bracken, C. (2002) An effective method for the discrimination of motional anisotropy and chemical exchange, *J. Am. Chem. Soc. 124*, 1852−1853.
40. Baldwin, J., and Chothia, C. (1979) Haemoglobin: the structural changes related to ligand binding and its allosteric mechanism, *J. Mol. Biol. 129*, 175−220.
41. Xu, C., Tobi, D., and Bahar, I. (2003) Allosteric changes in protein structure computed by a simple mechanical model: hemoglobin T ⇔ R2 transition, *J. Mol. Biol. 333*, 153−168.
42. Ramadas, N., and Rifkin, J. M. (1999) Molecular dynamics of human methemoglobin: the transmission of conformational information between subunits in an ab dimer, *Biophys. J. 76*, 1796−1811.
43. Tsai, C.-H., Fang, T. Y., Ho, N. T., and Ho, C. (2000) Novel recombinant hemoglobin, rHb(bN108Q), with low oxygen affinity, high cooperativity, and stability against autoxidation, *Biochemistry 39*, 13719−13729.
44. Tsai, C.-H., Shen, T.-J., Ho, N. T., and Ho, C. (1999) Effects of substitutions of lysine and aspartic acid for asparagine at β108 and of tryptophan for valine at α96 on the structural and functional properties of human normal adult hemoglobin: roles of $\alpha_1\beta_1$ and $\alpha_1\beta_2$ subunit interfaces in the cooperative oxygenation process, *Biochemistry 38*, 8751−8761.
45. Mouawad, L., Perahia, D., Robert, C. H., and Guilbert, C. (2002) New insights into the allosteric mechanism of human hemoglobin from molecular dynamics simulations, *Biophys. J. 82*, 3224−3245.
46. Balakrishnan, G., Tsai, C.-H., Wu, Q., Case, M. A., Pevsner, A., McLendon, G. L., Ho, C., and Spiro, T. G. (2004) Hemoglobin site-mutants reveal dynamical role of interhelical H-bonds in the allosteric pathway: time-resolved UV resonance Raman evidence for intra-dimer coupling, *J. Mol. Biol. 340*, 857−868.
47. Levy, A., Sharma, V. S., Zhang, L., and Rifkin, J. M. (1992) A new mode for heme-heme interactions in hemoglobin associated with distal perturbations, *Biophys. J. 61*, 750−755.
48. Fermi, G., Perutz, M. F., and Shaanan, B. (1984) The crystal structure of human deoxyhaemoglobin at 1.74 Å resolution, *J. Mol. Biol. 175*, 159−174.
49. Srinivasan, R., and Rose, G. D. (1994) The T-to-R transformation in hemoglobin: a reevaluation, *Proc. Natl. Acad. Sci. U.S.A. 91*, 11113−11117.
50. Mihailescu, M.-R., and Russu, I. M. (2001) A signature of the T→R transition in human hemoglobin, *Proc. Natl. Acad. Sci. U.S.A. 98*, 3773−3777.
51. Chang, C.-k., Simplaceanu, V., and Ho, C. (2002) Effects of amino acid substitutions at β131 on the structure and properties of hemoglobin: evidence for communication between $\alpha_1\beta_1$- and $\alpha_1\beta_2$-subunit interfaces, *Biochemistry 41*, 5644−5655.
52. Park, S.-Y., Yokoyama, T., Shibayama, N., Shiro, Y., and Tame, J. R. H. (2006) 1.25 Å resolution crystal structures of human haemoglobin in the oxy, deoxy and carbonmonoxy forms, *J. Mol. Biol. 360*, 690−701.
53. Lukin, J. A., Kontaxis, G., Simplaceanu, V., Yuan, Y., Bax, A., and Ho, C. (2004) Backbone resonance assignments of human

adult hemoglobin in the carbonmonoxy form, *J. Biomol. NMR 28*, 203−204.
54. Mueser, T. C., Rogers, P. H., and Arnone, A. (2000) Interface sliding as illustrated by the multiple quaternary structures of liganded hemoglobin, *Biochemistry 39*, 15353−15364.
55. Yang, D., and Kay, L. E. (1996) Contributions to conformational entropy arising from bond vector fluctuations measured from NMR-derived order parameters: application to protein folding, *J. Mol. Biol. 263*, 369−382.
56. Akke, M., Bruschweiler, R., and Palmer, A. G., III (1993) NMR order parameters and free-energy—an analytical approach and its application to cooperative Ca^{2+} binding by calbindin-D(9k), *J. Am. Chem. Soc. 115*, 9832−9833.
57. Lee, A. L., Kinnear, S. A., and Wand, A. J. (2000) Redistribution and loss of side chain entropy upon formation of a calmodulin-peptide complex, *Nat. Struct. Biol. 7*, 72−77.
58. Akke, M., Skelton, N. J., Kordel, J., Palmer, A. G., III, and Chazin, W. J. (1993) Effects of ion binding on the backbone dynamics of calbindin D9k determined by ^{15}N NMR relaxation, *Biochemistry 32*, 9832−9844.
59. Bracken, C., Carr, P. A., Cavanagh, J., and Palmer, A. G., III (1999) Temperature dependence of intramolecular dynamics of the basic leucine zipper of GCN4: implications for the entropy of association, *J. Mol. Biol. 285*, 2133−2146.
60. Fayos, R., Melacini, G., Newlon, M. G., Burns, L., Scott, J. D., and Jennings, P. A. (2003) Induction of flexibility through protein-protein interactions, *J. Biol. Chem. 278*, 18581−18587.
61. Arumugam, S., Gao, G., Patton, B. L., Semenchenko, V., Brew, K., and Van Doren, S. R. (2003) Increased backbone mobility in β-barrel enhances entropy gain driving binding of N-TIMP-1 to MMP-3, *J. Mol. Biol. 327*, 719−734.
62. Zidek, L., Novotny, M. V., and Stone, M. J. (1999) Increased protein backbone conformational entropy upon hydrophobic ligand binding, *Nat. Struct. Biol. 6*, 1118−1121.
63. Loh, A. P., Pawley, N., Nicholson, L. K., and Oswald, R. E. (2001) An increase in side chain entropy facilitates effector binding: NMR characterization of the side chain methyl group dynamics in Cdc42Hs, *Biochemistry 40*, 4590−4600.
64. Song, X.-j., Flynn, P. F., Sharp, K. A., and Wand, A. J. (2007) Temperature dependence of fast dynamics in proteins, *Biophys. J. 92*, L46−L48.

BI602654U